REPORT DOCUMENTATION PAGE

Form Approved OMB NO. 0704-0188

1. REPORT DATE (DD-MM-YYYY)	2. REPORT TYPE	3. DATES COVERED (From - To)
07-05-2015	Final Report	1-Jul-2014 - 31-Mar-2015

4. TITLE AND SUBTITLE

Final Report: Toward Theoretical Foundations of Resistive Force Theory of Granular-Structural Interaction, with Expansions to Flexible Locomotors

5a. CONTRACT NUMBER
W911NF-14-1-0205

5b. GRANT NUMBER

5c. PROGRAM ELEMENT NUMBER
611102

6. AUTHORS

Ken Kamrin

5d. PROJECT NUMBER

5e. TASK NUMBER

5f. WORK UNIT NUMBER

7. PERFORMING ORGANIZATION NAMES AND ADDRESSES

Massachusetts Institute of Technology (MIT
77 Massachusetts Ave.
NE18-901
Cambridge, MA 02139 -4307

8. PERFORMING ORGANIZATION REPORT NUMBER

9. SPONSORING/MONITORING AGENCY NAME(S) AND ADDRESS (ES)

U.S. Army Research Office
P.O. Box 12211
Research Triangle Park, NC 27709-2211

10. SPONSOR/MONITOR'S ACRONYM(S)
ARO

11. SPONSOR/MONITOR'S REPORT NUMBER(S)
65656-EG-II.1

12. DISTRIBUTION AVAILIBILITY STATEMENT

Approved for Public Release; Distribution Unlimited

13. SUPPLEMENTARY NOTES

The views, opinions and/or findings contained in this report are those of the author(s) and should not contrued as an official Department of the Army position, policy or decision, unless so designated by other documentation.

14. ABSTRACT

Granular Resistive Force Theory (RFT) is a reduced-order model inspired by analogous boundary-integral methods for Stokesian fluids. Despite its remarkable capability to predict experimental locomotion and force distributions on mobile bodies in granular media, there is no theoretical understanding for this behavior. Moreover, such a reduction is surprising given the highly nonlinear constitutive behavior of granular media. There could be a variety of reduced-order applications in various structure/granular interactions if a theoretical picture in explanation of RFT could be uncovered. Moreover, as with any accurate and sufficiently reduced model, RFT, once its limitations and

15. SUBJECT TERMS

Terramechanics, terradynamics, plasticity, soils, computation

16. SECURITY CLASSIFICATION OF:			17. LIMITATION OF ABSTRACT	15. NUMBER OF PAGES	19a. NAME OF RESPONSIBLE PERSON
a. REPORT	b. ABSTRACT	c. THIS PAGE			Kenneth Kamrin
UU	UU	UU	UU		19b. TELEPHONE NUMBER 617-715-4157

Standard Form 298 (Rev 8/98)
Prescribed by ANSI Std. Z39.18

Report Title

Final Report: Toward Theoretical Foundations of Resistive Force Theory of Granular-Structural Interaction, with Expansions to Flexible Locomotors

ABSTRACT

Granular Resistive Force Theory (RFT) is a reduced-order model inspired by analogous boundary-integral methods for Stokesian fluids. Despite its remarkable capability to predict experimental locomotion and force distributions on mobile bodies in granular media, there is no theoretical understanding for this behavior. Moreover, such a reduction is surprising given the highly nonlinear constitutive behavior of granular media. There could be a variety of reduced-order applications in various structure/granular interactions if a theoretical picture in explanation of RFT could be uncovered. Moreover, as with any accurate and sufficiently reduced model, RFT, once its limitations and backing is better understood, could be used as a reliable design-optimization tool to produce locomotors with optimal shapes, or tunable flexibility to improve efficiency of locomotion within granular media.

We have performed initial investigations of these questions. A systematic set of continuum simulations were conducted. In particular, we have determined that the RFT superposition principle arises naturally from full-field solutions of plasticity under Drucker-Prager yielding, the most commonly used plastic flow model for granular media in engineering. We find that the empirical input data used in RFT, fit from many experiments, in fact arises quantitatively from plastic flow solution, requiring only a friction coefficient and material density to solve. The results have motivated mathematical analyses to identify the approximations at play to achieve the desired model reduction. In parallel, a design-optimization protocol for wheeled locomotors in granular beds has been studied, based on numerical optimization of wheel shape. This effort has shown that under certain conditions, the natural curvature of a wheel tread under axle-bearing weight is proper to improve traction in soils.

Enter List of papers submitted or published that acknowledge ARO support from the start of the project to the date of this printing. List the papers, including journal references, in the following categories:

(a) Papers published in peer-reviewed journals (N/A for none)

Received	Paper

TOTAL:

Number of Papers published in peer-reviewed journals:

(b) Papers published in non-peer-reviewed journals (N/A for none)

Received	Paper

TOTAL:

Number of Papers published in non peer-reviewed journals:

(c) Presentations

Interaction of intruding objects within granular media using continuum modeling. H. Askari and K. Kamrin, APS March Meeting 2015

Number of Presentations: 1.00

Non Peer-Reviewed Conference Proceeding publications (other than abstracts):

Received Paper

TOTAL:

Number of Non Peer-Reviewed Conference Proceeding publications (other than abstracts):

Peer-Reviewed Conference Proceeding publications (other than abstracts):

Received Paper

TOTAL:

Number of Peer-Reviewed Conference Proceeding publications (other than abstracts):

(d) Manuscripts

Received Paper

TOTAL:

Number of Manuscripts:

Books

Received Book

TOTAL:

Received Book Chapter

TOTAL:

Patents Submitted

Patents Awarded

Awards

Graduate Students

NAME	PERCENT_SUPPORTED
FTE Equivalent:	
Total Number:	

Names of Post Doctorates

NAME	PERCENT_SUPPORTED
Hesam Asakri	1.00
FTE Equivalent:	**1.00**
Total Number:	**1**

Names of Faculty Supported

NAME	PERCENT_SUPPORTED	National Academy Member
Ken Kamrin	0.00	
FTE Equivalent:	**0.00**	
Total Number:	**1**	

Names of Under Graduate students supported

NAME	PERCENT_SUPPORTED
FTE Equivalent:	
Total Number:	

Student Metrics

This section only applies to graduating undergraduates supported by this agreement in this reporting period

The number of undergraduates funded by this agreement who graduated during this period: 0.00

The number of undergraduates funded by this agreement who graduated during this period with a degree in science, mathematics, engineering, or technology fields:..... 0.00

The number of undergraduates funded by your agreement who graduated during this period and will continue to pursue a graduate or Ph.D. degree in science, mathematics, engineering, or technology fields:..... 0.00

Number of graduating undergraduates who achieved a 3.5 GPA to 4.0 (4.0 max scale):..... 0.00

Number of graduating undergraduates funded by a DoD funded Center of Excellence grant for Education, Research and Engineering:..... 0.00

The number of undergraduates funded by your agreement who graduated during this period and intend to work for the Department of Defense 0.00

The number of undergraduates funded by your agreement who graduated during this period and will receive scholarships or fellowships for further studies in science, mathematics, engineering or technology fields: 0.00

Names of Personnel receiving masters degrees

NAME
Total Number:

Names of personnel receiving PHDs

NAME
Total Number:

Names of other research staff

NAME	PERCENT_SUPPORTED
FTE Equivalent:	
Total Number:	

Sub Contractors (DD882)

Inventions (DD882)

Scientific Progress

See Attachment

Technology Transfer

Title:

The origin of resistive force theory in granular materials

Authors:

Hesam Askari, Ken Kamrin*[1]

Affiliation:

Massachusetts Institute of Technology, 77 Massachusetts Ave., Cambridge, MA 02139

Abstract

The flowability of loose terrain under solid intrusion produces complex dynamics in problems ranging from geotechnical design to animal and vehicle locomotion. One approach is the Resistive Force Theory (RFT), a recent empirical tool for predicting granular-structure interaction. Its simplicity and effectiveness are surprising given the many complexities of granular flow, begging fundamental questions of why RFT works. We have found a link between RFT and plasticity theory, showing RFT arises solely from frictional yielding. Without any fitting, plasticity generates experimental RFT data, and reproduces RFT's foundational assumptions including spatial force superposition. Continuum dimensional analysis explains why RFT is more accurate in granular media than its older counterpart for viscous fluids, which instructs the development of RFT's in other media and for more diverse conditions.

One Sentence Summary:
We have discovered a fundamental link between the theory of granular plasticity and the as-yet empirical Resistive Force Theory of terradynamics.

Main Text:

Introduction -The interaction of solid objects with granular media is a common aspect of many engineering processes as seen in several examples of bio-locomotion and hydrodynamics [1, 2]. Interestingly, such a broad problem is not trivial to solve in granular materials due to the complexity of the response of the system and the many interaction forces that define the movement at the grain level, leaving explorations in this area to rely upon experimentally driven studies or numerical methods such as Discrete Element Method (DEM). Continuum modeling techniques that can accurately represent collective grain interactions on the macroscopic scale would be more efficient than DEM computationally, providing a route toward optimization in granular-structure interaction, and could yield new fundamental insights into the physics of granular resistance.

On the topic of interaction of granular material with intruding objects, attempts have been made mostly driven by experimental observations to describe this interaction. Despite the fact that a fundamental derivation is missing, a simple yet very effective empirical tool known as Resistive Force Theory (RFT) for granular materials has been proposed to approximate the forces on intruding objects moving through granular media. When coupled to the momentum balance equations, it provides a simple and predictive tool for simulating the locomotion of arbitrarily shaped moving bodies in loose terrain [2–4]. The simplicity of the theory and its predictive effectiveness are surprising in light of the complex, nonlinear, and oftentimes visibly nonlocal constitutive properties of granular media [5–9].

[1]kkamrin@mit.edu

A fundamental problem, then, is to determine why RFT works. Beyond theoretical concerns, understanding the origin of this rule could shed light on the requirements for its validity and the limits of its usage. In this paper we provide an answer to this question by supplying numerical and analytical evidence that RFT arises from the partial differential equations (PDE's) of frictional plasticity theory. To demonstrate this connection, we focus on dry granular material which is compliant to laboratory experiment and is representative of a wide class of flowable materials. *Resistive Force Theory* - RFT was initially developed to approximate the speed of swimming micro-organisms at low Reynolds numbers [10] by studying the thrust and drag of individually moving elements of its body. This method has been used extensively to study the hydrodynamics and mobility of cells as reviewed in [11]. In the study of granular media, a similar notion arose much more recently, when in experimental studies of arbitrarily-shaped intruders moving in granular beds, it was determined that the resistive force against intruder motion is rather well represented by a simple *superposition rule* [4]; the intruder boundary can be decomposed into a connected collection of differential planar elements and the total resistive force is deemed equal to the sum of the resistive forces on each plane as if it was moving steadily on its own. RFT can be used in general 3D setups, but for concreteness, let us consider now the case of a quasi-2D intruder having some thickness D which displaces in the xz-plane (gravity points in $-\hat{z}$ direction, $z = 0$ represents the sand surface) and whose cross-section also lies in the xz-plane. For any subset S of the leading surface of the intruder, RFT states the resistive force on S will obey

$$(f_x, f_z) = \int_S \big(\alpha_x(\beta,\gamma),\ \alpha_z(\beta,\gamma)\big)\ H(z)\ |z|\ dS \tag{1}$$

where β is the orientation angle (attack angle) of the differential surface element and γ is the angle of the velocity angle (intrusion angle) of the surface element, both measured from the horizontal. The Heaviside function, $H(z)$, removes resistive force above the granular level and increases resistance with depth to reflect the increase in granular pressure with depth. The key constitutive ingredient in the theory is the selection of the two functions α_x and α_z, which is done empirically by fitting experimental force data on intruding flat plates under various γ and β conditions.

Continuum Modeling - Frictional plasticity models based on the Mohr-Coulomb (MC) yield criterion or Drucker-Prager (DP) criterion are the most commonly used granular continuum models for predicting the deformation of a body of grains. We choose to study the DP yield criterion in this paper as it is simpler to implement in 3D, and in 2D the theory matches MC. We will make two important choices in closing the system of constitutive equations: (i) we choose a non-associative flow rule corresponding to incompressible flow during yielding, to emulate an immediate approach to a critical state [5] of volume-conserving flow, and (ii) we append an 'opening rule' to the system to remove granular stress when a material element attempts to enter a state of tension, as granular media naturally disconnects when a tensile state is attempted. Open states often occur temporarily in the wake of a moving intruder, before material from above collapses onto the material back down (see Supplemental Materials for more details). The bare-bones granular flow model described above does not account for rate-sensitivity, strain-dependent strength/porosity, fabric anisotropy during flow, or nonlocal effects based on particle size, which are all known to exist.

The strain-rate tensor is defined from the spatial velocity field, v_i, by $D_{ij} = (\partial v_i/\partial x_j + \partial v_j/\partial x_i)/2$. We define the scalar (equivalent) shear-rate as $\dot{\gamma} = \sqrt{2D'_{ij}D'_{ij}}$ where $D'_{ij} = D_{ij} - \delta_{ij}D_{ii}/3$ is the strain-rate deviator. Assuming that the Cauchy stress, σ_{ij}, is co-directional with the strain-rate, the DP criterion reduces to

$$\sigma_{ij} = -P\delta_{ij} + 2\mu_c P D'_{ij}/\dot{\gamma} \quad \text{if} \quad \dot{\gamma}, P > 0. \tag{2}$$

In the above, μ_c is a constant internal friction coefficient and P is the isotropic pressure. Whenever

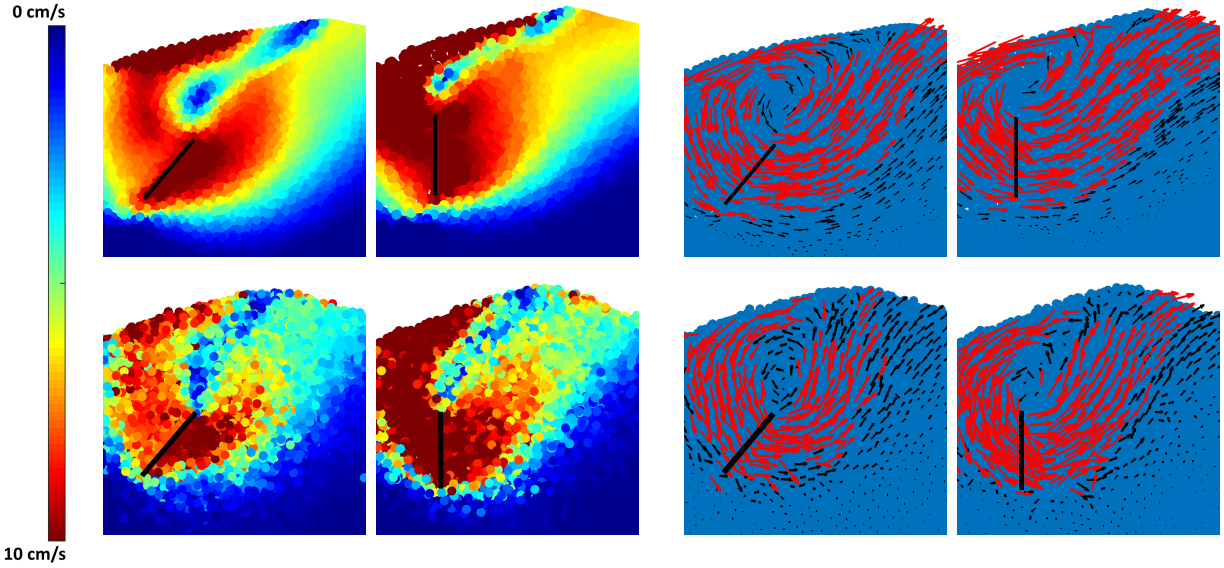

Figure 1: Speed (left two columns) and velocity directions (right two columns) due to the motion of a buried flat intruder of different orientations moving to the right. Top row: FEM simulations of the continuum model. Bottom row: DEM simulations of [3]. Velocity arrows corresponding to regions moving at the speed of more than 5 cm/s are as red.

$\dot{\gamma}, P > 0$ we assume incompressibie plastic flow ($D_{ii} = 0$) such that the material density ρ remains at a chosen 'dense' value ρ_c. Whenever $\rho < \rho_c$, we set $\sigma_{ij} = 0$ to represent granular disconnection. To provide a stress in rigid zones, where $\dot{\gamma} = 0$ and $P > 0$, and to aid in implementing the pressure constraints numerically, we include a small elastic part to the deformation [12]; as long as the elastic stiffness is sufficiently high the observed plastic flow behavior is unaffected, a point we verified directly in our simulations. Momentum balance, $\partial\sigma_{ij}/\partial x_j + \rho g_i = \rho\dot{v}_i$, closes the system for arbitrary boundary value problems, where g_i is the acceleration of gravity and the superscript dot represents the Lagrangian time derivative.

FEM Results - The model just described is numerically implemented in 3D using Abaqus/Explicit [13]. The constitutive relation is inputted as a custom VUMAT subroutine. We first consider problems with plane-strain symmetry. We use second order explicit tetrahedral elements in Abaqus package to discretize the granular material space into a finite element mesh. The meshed space is a row of single element thickness and consequently resembles plane strain condition. On any container edge, no-penetration conditions are applied. Gravity is applied to obtain the proper depth-dependent pressure distribution before intruder motion begins. We model the intruder as a rigid surface within the granular body by assigning corresponding planar nodes to move as a rigid body at a constant rate. This resembles a fully rough surface due to the no-slip condition, no penetration condition. We use sufficiently refined second-order elements to maintain solution accuracy. Sample flow directions and velocity distributions within the granular material obtained by FEM are shown in Fig. 1 and compared to the DEM results in the literature [3]. It is worthwhile to note that at the intruder interface, grains naturally tend to slide or rotate, so our no-slip condition is hard to physically replicate. But this approach relinquishes the need to define a complex contact routine which brings in additional contact parameters.

To perform a quantitative analysis of the approach and to establish the connection between frictional plasticity and RFT, we repeated the method described above on an intruder at attack angles β and intrusion angles γ ($0 < \beta, \gamma < \pi$). The drag and lift forces acting on the plate are

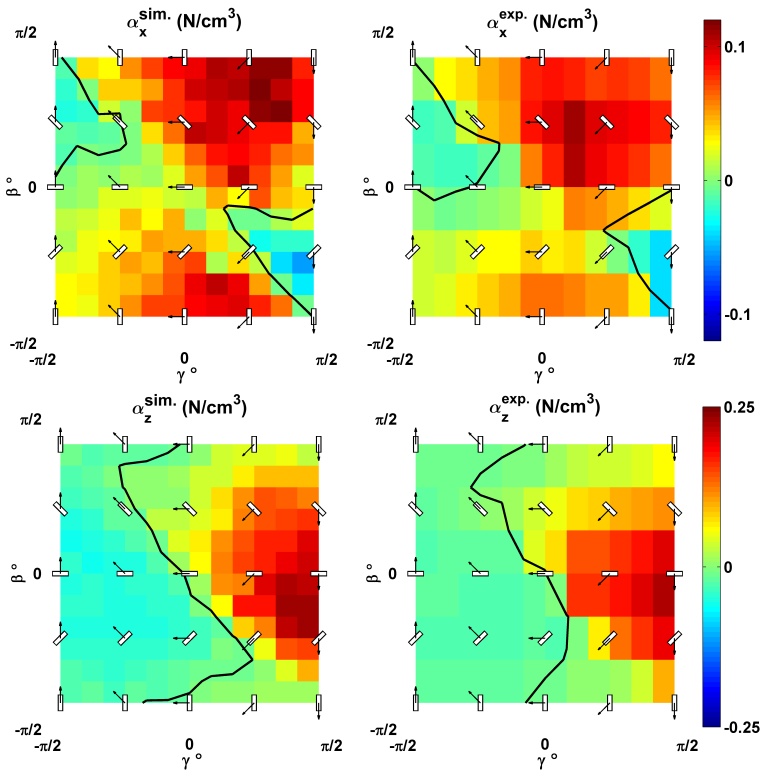

Figure 2: RFP's obtained from FEM simulations with frictional plasticity ('sim.' superscript), compared against experimental RFP's ('exp.' superscript) from [2] . Solid black line shows the zero contour.

then converted to the two functions α_x and α_z, which is done by averaging over a period of time after plastic deformation is well developed. We use the properties of loose packed 3mm glass beads as reported in [2]: the friction coefficient is $\mu_c = 0.38$ based on their repose angle calculation, the density is $\rho = 2.6$ g/cm^3, and the packing fraction of 0.63. As plotted in Fig.2, the resistive force plots (RFP) of α_x and α_z are strikingly similar to the experimentally obtained RFPs reported in [2] for loose-packed 3mm glass beads that show quantitative agreement. Furthermore the zero contour lines in the numerical RFPs follow the same path as that of the experimental RFPs. The only noticeable difference between the two sets of figures is observed in the location of maximum drag force in the ($\alpha_x^{\text{sim.}}$) plot, which can be attributed to the no-slip boundary condition used in the simulations. What is more remarkable about this figure is that no fitting parameters are used in the constitutive model, only the physically measurable quantities of density, repose angle and packing fraction.

These plots are also noticeably accurate in reproducing the resistive force distribution of an arbitrarily shaped object moving within continuum granular material. For instance, in Fig. 3, the distribution and resultant forces acting on circular and diamond-shaped intruders is obtained directly by FEM and compared with those predicted by the FEM-generated RFP's under the form of Eq. 1. These illustrations show the extent of the validity of the superposition rule of RFT and further show the connection between frictional plasticity and RFT. Though some errors are observed at the edges, the distribution and total forces are closely comparable. Normal and shear stresses on the perimeter of the leading edge of the circular object show a very close match in the bottom quarter, but deviations pick up in the top quarter which is attributed to the no-slip condition. The material at the backward inclined surface tends to slide in reality, where in case of our simulation this movement

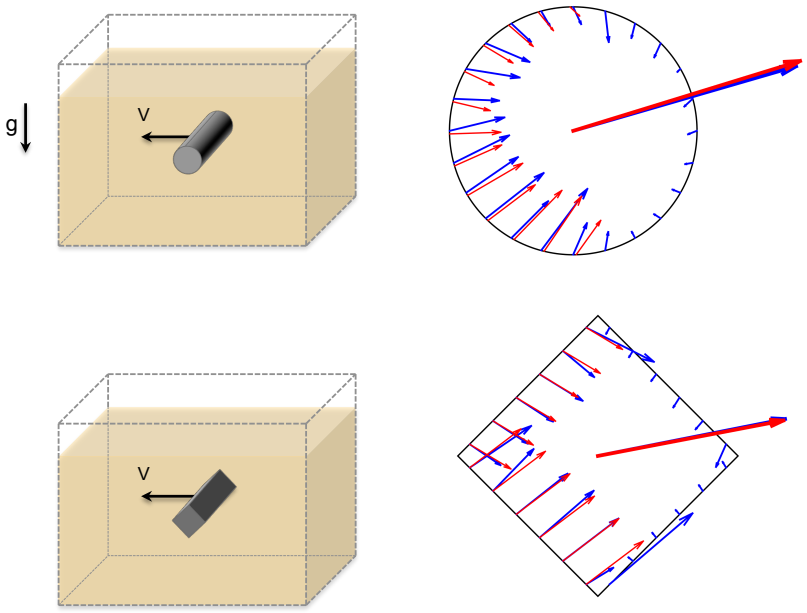

Figure 3: Distribution of force on the perimeter of infinitely long moving objects calculated from FEM simulation (→), compared to predictions from RFT obtained by simulation (→). Net resistive force shown at the center of the object.

is confined due to no slip condition.

Exploration of superposition in 3D - Equation 1 can be extended naturally to include the out-of-plane dimension, backed by experiments [2] that have verified that surfaces whose shapes vary in the y direction also maintain the superposition principle. To assess the RFT superposition principle in 3D, we employ our continuum model to study a sequence of horizontal motions of a buried V-shaped intruder. There are natural limitations on the superposition principle regarding the curvature, angularity or orientation of the intruding object. For example, if the V angle is too close to zero, i.e. the two wings of the V nearly coalesce, RFT will be wrong by a factor of two since one wing is completely blocked by the other. To study RFT in its plausible regime, we hence limit our attention to an obtuse V geometry, with angle fixed at 135° that ought to be within the limits of the theory. The intruder is located at depth of 0.75m measured from the center of its spine and each wing is a 0.2 x 0.2m square.

We consider the case where the intruder is moving as a one piece object and we record its forces in three dimensions. Then we run two new simulations, one for each wing of the intruder, where the wing is simulated as a separate single plate maintaining its same exact same alignment, positioning, and motion that it had when it partook in the group V motion. We consider both vertically and horizontally aligned intruder cases, varying the orientation angle ϕ denoting a pitching angle (in vertical case) or yawing angle (in horizontal case), see Fig. 4. Both cases engage in considerable drag force in the direction of motion as expected. The vertically aligned intruders experiences no lateral force due to symmetry, with lift forces that switch sign due to the plowing. The horizontal intruder experiences somewhat steady lift force, but the lateral forces vary considerably for similar lift of the vertical intruder.

We evaluate RFT by comparing the forces obtained directly by FEM of the V intruder (Fig. 4 solid lines) with the forces obtained by summation of contributions from individually moving component plates (Fig. 4 dashed lines). This comparison shows that the theory generally works

very well in 3D. We find the agreement is more pronounced when a particular wing is positioned such that there is less interaction between the flow-fields stemming from each plate. The agreement is roughly in the same range as the deviations observed in past granular RFT experiments [3, 14]. For certain orientations, the disagreement is due to a 'shadowing' effect caused by the leading wing on the trailing wing. For instance at 0° a good agreement between group and individual forces is observed for the vertically aligned intruder. One can expect the flow fields of both wings to point in the same direction (See Fig. 1) and little effect should be expected from the cross-interaction of the fields. But once the same object is rotated by 90°, these fields would interact and therefore the disagreement in forces increases in all components. For this 3D study there are no analogous experimental tests in the literature to verify the FEM findings. But the results shown in Fig. 4 suggest that for 3D objects that do not contain sharp acute angles and their geometry does not shadow parts of their own perimeter, reasonable results should be expected if RFT is used.

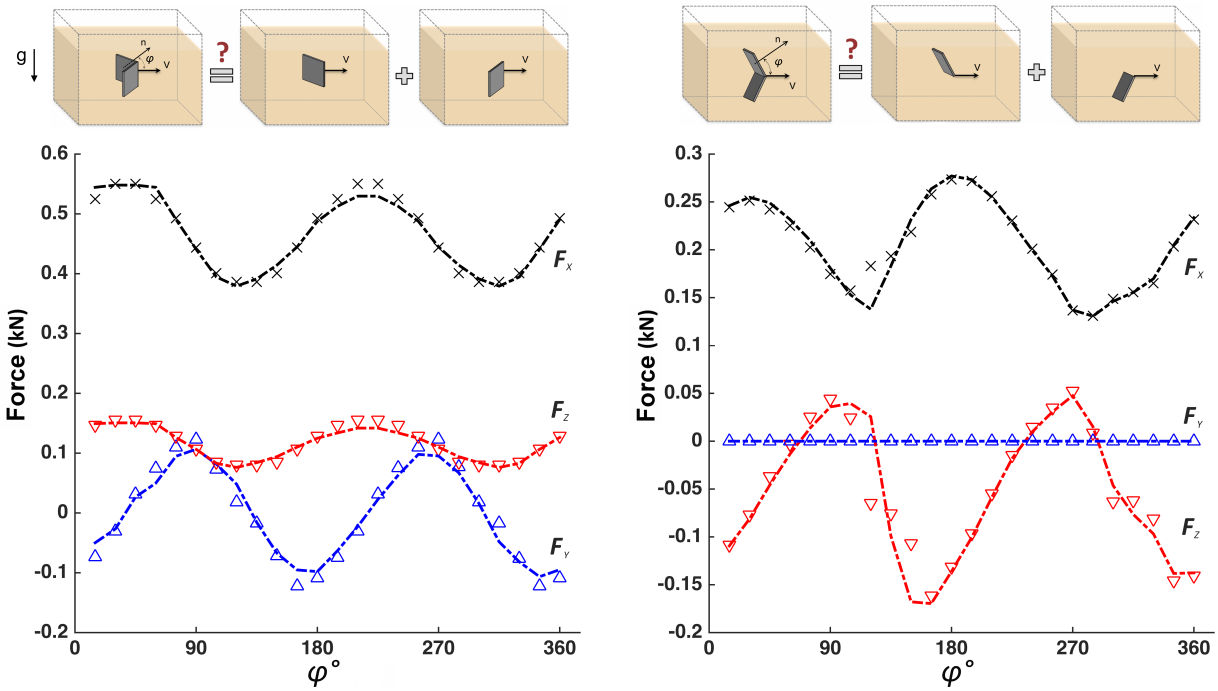

Figure 4: The drag force, F_x, acting on a rightward moving submerged 'V' intruder (×), and the components of lift, F_z (▽), and lateral force, F_y (△), compared with superposition values (dashed) at various orientation angles, φ, for horizontal (left) and vertical (right) intruder alignments.

Mathematical explanation - The results thus far have demonstrated numerically that the hypotheses of RFT emerge relatively strongly from the continuum equations of frictional plasticity. To provide more of an explanation as to *why* the continuum equations replicate RFT, we consider the following example. As delineated earlier, exact solutions to the continuum plasticity system are highly nontrivial to obtain, but the example we highlight below can be proven using dimensional analysis to collapse exactly to RFT.

Consider a large, quasi-2D (of arbitrary out-of-plane width D), semi-infinite bed of our continuum plastic media. Suppose a straight intruder is inserted into the media at an angle β from the horizontal, such that L of its length is submerged. It is then translated at a speed v in a direction angled γ from horizontal, producing an assumed quasi-static, plane-strain motion of the material. At the moment the motion begins, the total resistive force $\mathbf{F}$ on the intruder can be calculated. If the

calculation is repeated for a slightly longer intruder, of submerged length $L + dl$, we can ask how much extra resistive force is there, or equivalently, what is $d\mathbf{F}/dl$? The continuum model inputs and boundary conditions imply that the answer can only depend on β, γ, L, the granular areal weight density $\rho g D$, the internal friction μ_c, and perhaps a wall friction coefficient μ_w between the intruder and the material. Let the units of length, time, and mass be [Length] $= L$, [Time] $= L/v$ and [Mass] $= \rho g D * L * (L/v)^2$ respectively. The dimensionless groups are then $(d\mathbf{F}/dl)/(\rho g D * L^2)$, β, γ, μ_c, and μ_w. It therefore follows that

$$\frac{d\mathbf{F}}{dl} = \rho g D L \; \boldsymbol{\psi}(\beta, \gamma, \mu_c, \mu_w) = |z| D \; \boldsymbol{\Psi}(\beta, \gamma, \mu_c, \mu_w) \tag{3}$$

where the right equality uses $|z| = L \sin\beta$. By integrating, we find Eq.3 gives the general form of the RFT (see Eq.1) where the components of the function $\boldsymbol{\Psi}$ are precisely the lift and drag functions $\alpha_z(\beta, \gamma)$ and $\alpha_x(\beta, \gamma)$, which depend on the material properties and intruder roughness through μ_c and μ_w.

While instructive, the above shows only that RFT is exact in the specific case described and does not explain its general effectiveness for curved, submerged surfaces. In more general geometries, we hypothesize that the reason for continued RFT-type superposition may be linked to the fact that the equations of frictional plasticity for 2D, quasi-static, rigid-plastic problems become a hyperbolic system in space. The stress characteristics extend from boundaries along lines saturating $|\tau|/P \leq \mu_c$, that form the 'slip-lines' [15]. This produces domains of dependence in the material in a sense that stresses in certain zones can be attributed to the traction on a specific part of the surface of the intruder. This is in sharp contrast to viscous fluids, for example, in which the equations are elliptic. Experimentally, superposition tends to work better in granular media than it does for viscous fluids [16], which is particularly ironic given that RFT was initially developed for viscous drag [17]. Using an analogous dimensional analysis as above but this time assuming a viscous fluid rheology leads to $d\mathbf{F}/dl = |z| \, D \, \boldsymbol{\Psi}(\beta, \gamma, \mu_w, vz/\nu)$ which confirms that the form of the force function does not reduce to the superposition form of Eq.3 since viscosity brings in an additional velocity and depth dependence through a dimensionless group vz/ν for ν the kinematic viscosity. Further details of the viscous vs granular analysis can be found in the Supplemental Materials.

We have shown that the basis of the granular superposition rule and the other hypotheses of RFT, arise in full from the most basic law of continuum frictional plasticity. We have verified this point directly in plane-strain and full 3D problems. Moreover, the plasticity system, when fit to the repose angle of the physical media of [2], quantitatively replicates the empirical input data that was previously used for RFT. We have identified how the exact form of RFT arises in a model problem, based solely on dimensional analysis. In so doing, we have also explained why RFT works better in granular matter than in viscous fluids. This new fundamental understanding paves the path forward to better understand and derive RFT's for other flowable materials, or apply the method in systems that might be difficult to approach otherwise experimentally such as the modeling of terradynamics in micro-gravity. For example, using a similar analysis to the one above, certain cohesive media may also possess an RFT describing forces on moving locomotors; see Supplemental Materials 4.2. By rooting RFT in the fundamental plasticity equations we now have a clear mechanical framework to understand the various parameters in RFT as well as to discern the circumstances that diminish the accuracy of the model.

References and Notes:

References

[1] M. H. Dickinson, *et al.*, *Science* **288**, 100 (2000).

[2] C. Li, T. Zhang, D. I. Goldman, *Science* **339**, 1408 (2013).

[3] Y. Ding, N. Gravish, D. I. Goldman, *Physical Review Letters* **106**, 028001 (2011).

[4] R. D. Maladen, Y. Ding, P. B. Umbanhowar, A. Kamor, D. I. Goldman, *Journal of The Royal Society Interface* **8**, 1332 (2011).

[5] A. Schofield, P. Wroth (1968).

[6] K. Kamrin, *Int. J. Plasticity* **26**, 167 (2010).

[7] K. Kamrin, G. Koval, *Phys. Rev. Lett.* **108**, 178301 (2012).

[8] D. L. Henann, K. Kamrin, *Proceedings of the National Academy of Sciences* **110**, 6730 (2013).

[9] W.-F. Chen, *Limit analysis and soil plasticity* (Elsevier, 2013).

[10] J. Gray, G. Hancock, *Journal of Experimental Biology* **32**, 802 (1955).

[11] E. Lauga, T. R. Powers, *Reports on Progress in Physics* **72**, 096601 (2009).

[12] R. Hill, *Journal of the Mechanics and Physics of Solids* **5**, 66 (1956).

[13] Dassault Systèmes Simulia, Providence, RI, *Abaqus Reference Manuals*, 6th edn. (2011).

[14] D. I. Goldman, *Reviews of Modern Physics* **86**, 943 (2014).

[15] R. M. Nedderman, *Statics and kinematics of granular materials* (Cambridge University Press, 2005).

[16] B. Rodenborn, C.-H. Chen, H. L. Swinney, B. Liu, H. Zhang, *Proceedings of the National Academy of Sciences* **110**, E338 (2013).

[17] J. Lighthill, *Mathematica) Biofluiddynamics* (SIAM, 1975).

The origin of resistive force theory in granular materials
(Supplemental materials)

Hesam Askari, Ken Kamrin
Massachusetts Institute of Technology

The goal of this supplemental material is to provide details about the modeling technique and calculations presented in the main text. We describe different components of the finite element approach and the corresponding parameters followed by a more detailed discussion on the dimensional analysis.

1 Numerical solution procedure

1.1 Elasticity-augmented constitutive relation

As outlined in the main paper, we describe the deformation behavior of the granular material by using a non-hardening Drucker-Prager (DP) yield criterion (constant μ_c). When implementing the model, we assume a small portion of the deformation is elastic, which closes the system mathematically in regions of non-flowing material, and provides a natural route to implementing the pressure constraints described. The model then takes the form of a simple hypo-plastic formulation. At any time, the deformation gradient F_{ij} is used to construct the velocity gradient $\partial v_i/\partial x_j = \dot{F}_{ik}F^{-1}_{kj}$, which is further divided into a symmetric stretching component D_{ij} and anti-symmetric spin component W_{ij}. The dot represents the Lagrangian time derivative. The stretching is further decomposed into elastic and plastic parts $D_{ij} = D^e_{ij} + D^p_{ij}$. Denoting the elastic shear and bulk moduli of the granular material by G and K respectively, the constitutive relationship for the stress evolution of dense material (i.e. $\rho \geq \rho_c$) is established by a Jaumann objective rate form as follows:

$$\begin{cases} \sigma_{ij} = 0, & \text{if } \rho < \rho_c \\ \dot{\sigma}_{ij} - W_{ik}\sigma_{kj} + \sigma_{ik}W_{kj} = KD^e_{kk}\delta_{ij} + 2G(D^e_{ij} - D^e_{kk}\delta_{ij}/3), & \text{if } \rho \geq \rho_c \end{cases} \tag{1}$$

where σ_{ij} is the Cauchy stress as described in the main paper which is divided into a hydrostatic pressure part $\bar{\sigma} = \sigma_{kk}/3 = -P$ and a deviatoric part $\sigma'_{ij} = \sigma_{ij} - \bar{\sigma}\delta_{ij}$. This relationship warrants that the material is stress-free if density falls below a certain critical density ρ_c which is indicative of a disconnected or 'open state' of the material. Further discussion about this condition is followed in section 1.3 of this supplement.

1.2 Update step

The numerical scheme is a variant of the radial return algorithm [1] . It starts each step by assuming a purely elastic step, i.e. $D^p_{ij} = 0$, under Equation 1, which updates the stress to a "trial stress" (σ^{tr}_{ij}). If the trial stress results in an equivalent shear stress $\bar{\tau}^{tr} = \sqrt{\sigma^{tr'}_{ij}\sigma^{tr'}_{ij}/2}$ that is less than $\mu_c P^{tr}$, it is accepted as the updated stress. If not, it is then adjusted as shown in Figure 1. In this figure, σ^t_{ij} is the stress state at the beginning of the step. Since $P^{tr} = P^{t+\Delta t}$ due to the isochoric plastic flow

assumption, the effective shear stress $\bar{\tau}$ should reduce following a constant pressure route to reside on the yield surface and $\sigma_{ij}^{t+\Delta t}$, the stress state at the end of increment, is updated accordingly. This essentially represents usage of a tangent modulus to return the trial stress state σ_{ij}^{τ} back to the yield surface at the end of the increment [1].

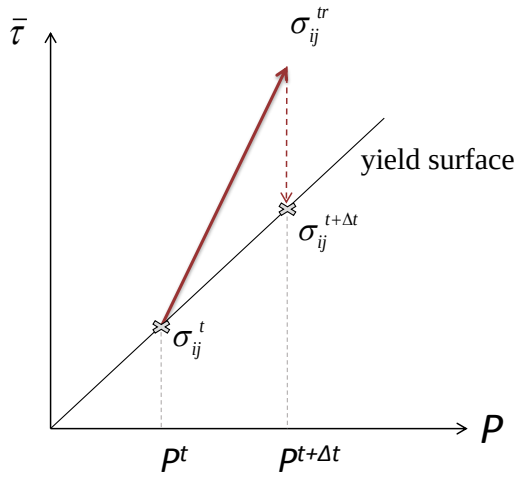

Figure 1: Projection of stresses to the yield surface.

$$\sigma_{ij}^{t+\Delta t} = \sigma_{ij}^{'tr}(\mu_c P^{t+\Delta t}/\bar{\tau}^{tr}) - P^{t+\Delta t}\delta_{ij} \tag{2}$$

Note that the values of P and $\bar{\tau}$ should be updated after this projection. Adjustments should also be made if the material is stretched beyond a critical density as described below.

1.3 Simultaneous dense and disconnected matter

Following [2], the opening rule is implemented by tracking the Jacobian ($\det(F_{ij})$) at each integration point. If the initial local density at a material point is denoted by ρ_0, then its density in deformed state is $\rho = \rho_0/\det(F_{ij})$. If the Jacobian exceeds unity, the local density at the deformed stage is reduced. Once the deformed density is smaller than critical density ρ_c the material point is flagged to behave locally as open state i.e. stress free deformation. In all our simulations, we begin by assuming $\rho_0 = \rho_c$, i.e. a granular assembly barely in contact, and turn gravity on in a following step, which causes the material to compress elastically a small amount.

In the case of an flat plate traveling within granular material, one would expect that behind the intruder, the free space caused by movement of the object would cause open states in its wake. Consequently the open material above the region should fall down and fill the cavities caused by the intruder movement as shown in density plot in 2. The open states in the back of the intruder are more or less persistent after reaching steady-state deformation while in the front there are isolated areas that show a limited amount of reduction in density. As expected, the figure shows these locations form in the trailing path of the intruder.

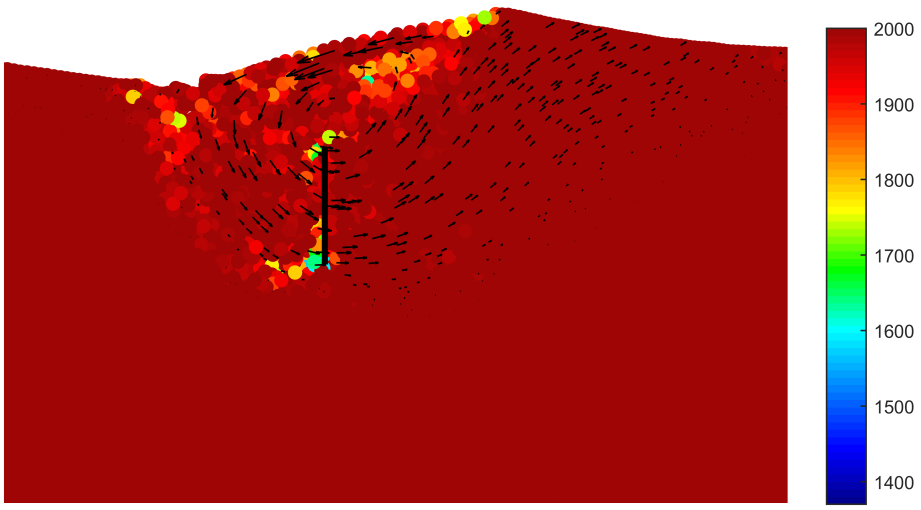

Figure 2: Plot of the local density in the granular bed in the wake of a flat vertical intruder moving rightward using FEM. Densities below $\rho_c = 2000$ kg/m^3 denote disconnected material in an 'open state'.

2 Dimensional analysis

Here we extend and clarify the dimensional analysis examples presented in the main paper with a complete description to study the form of resistive forces in granular materials and to contrast it with viscous fluids.

2.1 Granular material

Assume a perfectly plastic bed of grains ($K, G \to \infty$) and a straight intruder of out-of-plane width D and length L. Let the friction coefficient for the granular media and the wall friction coefficient for the intruder be μ_c and μ_w respectively, and the weight density of the material be ρg. Assume quasi-static motion of the intruder.

2.1.1 Intruder in the vertical plane

Consider a cross-sectional slice of the above mentioned box as shown in figure 3 in plane strain conditions. The intruder travels at speed v with intrusion angle of γ, pushing the material in front. The intruder is oriented at angle β with its length of L being in contact with the granular material. We assume plasticity is reached instantaneously. If the force is denoted as $\mathbf{F}$, then the rate of change in force with respect to change in length, denoted by $d\mathbf{F}/dl$, represents the deviation in the force if the intruder were extended slightly longer by length of dl. Based on the assumptions above, $d\mathbf{F}/dl$ can only depend on $\beta, \gamma, L, v, \rho g D, \mu_c$ and μ_w. The units of length, time and mass are represented as $[L] = L, [T] = L/v, [M] = \rho g D * L * L^2/v^2$ respectively and the dimensionless force denoted by tilde is obtained as:

$$\tilde{\mathbf{F}} = \frac{\mathbf{F}}{[M][L]/[s]^2} = \frac{\mathbf{F}}{\rho g D \frac{L^3}{v^2} L \frac{v^2}{L^2}} = \frac{\mathbf{F}}{\rho g D L^2} \tag{3}$$

Therefore it follows that $d\mathbf{F}/dl = \rho g D L\ \boldsymbol{\psi}(\beta, \gamma, \mu_c, \mu_w)$. Substituting $|z| = L \sin\beta$, we can write:

$$\frac{d\mathbf{F}}{dl} = \rho g D L\ \boldsymbol{\psi}_{vert}(\beta, \gamma, \mu_w, \mu_c) \to \frac{d\mathbf{F}}{dl} = |z|\ D\ \boldsymbol{\Psi}_{vert}(\beta, \gamma, \mu_w, \mu_c) \tag{4}$$

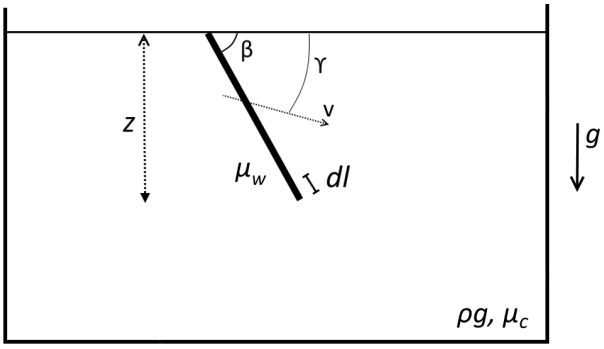

Figure 3: Arbitrarily oriented vertical intruder set into motion in an arbitrary direction. Plane strain conditions.

which is the differential form of the RFT equation; ρg has been absorbed in to the definition of $\mathbf{\Psi}_{vert}$. Here the components of the function $\mathbf{\Psi}_{vert}$ precisely define $\alpha_x(\beta, \gamma)$ and $\alpha_z(\beta, \gamma)$ of Eq 1 in the main text.

2.1.2 Horizontal intruder

Consider the same configuration described above, but this time for a horizontally aligned intruder. This time, we consider a horizontal cross-section at depth $z > 0$ passing through the intruder. By making the simplifying approximations that (i) that the pressure is a linear function of depth, and (ii) flow is contained within the cross-section, we can identify a pseudo-cohesion parameter in the equations, defined as $\mu_c \rho g z D$, which emerges as a constant effective material strength per length within the cross-section. Therefore $d\mathbf{F}/dl$ in this case depends on $\theta, \omega, L, v, \mu_c \rho g z D, \mu_c$, and μ_w. We choose dimensional units in this configuration to be $[L] = L, [T] = L/v, [M] = \mu_c \rho g z D * L^2/v^2$ and the dimensionless force is:

$$\tilde{\mathbf{F}} = \frac{\mathbf{F}}{[M][L]/[s]^2} = \frac{\mathbf{F}}{\mu_c \rho g z \frac{L^2}{v^2} L \frac{v^2}{L^2}} = \frac{\mathbf{F}}{\mu_c \rho g z L} \tag{5}$$

Therefore it follows similarly that:

$$\frac{d\mathbf{F}}{dl} = \mu_c \rho g z D \; \boldsymbol{\psi}_{hor}(\theta, \omega, \mu_w, \mu_c) \rightarrow \frac{d\mathbf{F}}{dl} = |z| \;\; D \; \mathbf{\Psi}_{hor}(\theta, \omega, \mu_w, \mu_c) \tag{6}$$

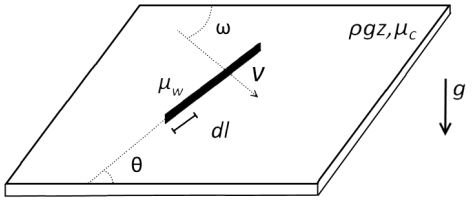

Figure 4: Horizontal intruder - plane view perpendicular to gravity.

This analogy creates a correlation between the effects of depth in cohesion-less material and arbitrary cohesion parameter in a cohesive material.

2.2 Stokes flow: Intruder in a vertical plane

For viscous incompressible slow-regime flow, the general Navier-Stokes equation reduces to Stokes equation as $-\nu\rho(\partial^2/\partial x_j^2)v_i - (\partial/\partial x_i)P + f_i = 0$ with condition $\partial v_i/\partial x_i = 0$ to enforce incompressibility. Here, v is velocity, P is pressure, ν is kinematic viscosity and f is body force. For the case of vertical intruder, the only body force is the gravity and the boundary condition and properties of the material imply that the forces depend on $\alpha, \beta, v, L, z, \rho g D, \nu$. The main units are again found as $[L] = L, [T] = L/v, [M] = \rho g D * L * (L/v)^2$, then the dimensionless viscosity is found by $\tilde{v} = \nu/vL$ and the dimensionless force is:

$$\tilde{\mathbf{F}} = \frac{\mathbf{F}}{[M][L]/[s]^2} = \frac{\mathbf{F}}{\rho g \frac{L^3}{v^2} L \frac{v^2}{L^2}} = \frac{\mathbf{F}}{\rho g L^2} \tag{7}$$

Consequently, the force on the intruder is found as:

$$\frac{d\mathbf{F}}{dl} = \rho g L \ \boldsymbol{\psi}_{visc}(\beta, \gamma, \mu_w, \frac{\nu}{vL}) \rightarrow \frac{d\mathbf{F}}{dl} = |z| \ \boldsymbol{\Psi}_{visc}(\beta, \gamma, \mu_w, \frac{\nu}{vz}) \tag{8}$$

As seen above, the dimensionless viscosity group carries z-dependence inside the function $\boldsymbol{\Psi}_{visa}$. This dependence enables the correlation to deviate from a purely linear correspondence on z as seen in RFT for granular material. A similar result occurs for the case where the object is horizontally oriented.

References

[1] J. C. Simo, R. L. Taylor, *Computer methods in applied mechanics and engineering* **48**, 101 (1985).

[2] S. Dunatunga, K. Kamrin, *arXiv preprint arXiv:1411.5447* (2014).